SOLVING THE CHAN-VESE MODEL BY A MULTIPHASE LEVEL SET ALGORITHM BASED ON THE TOPOLOGICAL DERIVATIVE

LIN HE* AND STANLEY OSHER †

Abstract. In this work, we specifically solve the Chan-Vese active contour model by multiphase level set methods. We first develop a fast algorithm based on calculating the variational energy of the Chan-Vese model without the length term. We check whether the energy decreases or not when we move a point to another segmented region. Then we draw a connection between this algorithm and the topological derivative, a concept emerged from the shape optimization field. Furthermore, to include the length term of the Chan-Vese model, a preprocessing step is taken by using nonlinear diffusion. Numerical experiments have demonstrated the efficiency and the robustness of our algorithm.

Key words. Image Segmentation, Level Set Methods, Chan-Vese model, Topological Derivative.

1. Introduction. Image segmentation, an important problem in image analysis, is to partition a given image into disjoint regions, such that the regions correspond to the objects in the image. There are a wide variety of approaches to the segmentation problem. One of the popular approaches is active contour models or snakes, first introduced by Terzopoulos et al. [27, 26]. The basic idea is to start with a curve around the object to be detected, the curve moves towards to its interior normal and has to stop on the boundary of the object. The main drawbacks of the orginal snakes are their sensitivity to initial condtions and the difficulties associated with topological transformations. Caselles et al. [5] thus introduced the first level set formulation for the geometric active contour model in a non-variational setting (see also Malladi et al. [18]) and later in a variational form [6] (cf. Kachenassamy et al. [13]). A major advantage of the level set approach [21] is the ability to handle complex topological changes automatically. However, all above active contour models are depending on the gradient of the given image to stop the evolution of the curve. Therefore these models can only detect objects with edges defined by a gradient.

Based on the Mumford-Shah functional [19] for segmentation, Chan and Vese [7, 28] proposed a new level set model for active contours to detect objects whose boundaries are not necessarily defined by a gradient. In this paper, we will focus on solving this model. We denote the given image $f : D \to \mathbb{R}$, where $D \in \mathbb{R}^2$ is an open and bounded set. We let Ω, an open subset of D, to be the detected objects. Thus we write the boundary of the detected objects as $\partial\Omega$. The Chan-Vese model is to minimize the following variational functional,

$$F(\Omega, c_1, c_2) = \min_{\Omega, c_1, c_2} \int_{\Omega} (f - c_1)^2 \, dx + \int_{D \setminus \Omega} (f - c_2)^2 \, dx + \mu \int_{\partial\Omega} ds, \tag{1.1}$$

where $\mu > 0$ is the so called length parameter chosen by the user. To solve this minimization problem (1.1), the level set method [21] is used. A level set function $\phi(x)$ is represented by the region Ω as follows,

$$\phi(x) \begin{cases} > 0 & \text{if } x \in \Omega, \\ < 0 & \text{if } x \in D \setminus \bar{\Omega}. \end{cases}$$

*Johann Radon Institute for Computational and Applied Mathematics, 4040 Linz, Austria, lin.he@ricam.oeaw.ac.at

†UCLA Mathematics Department, Box 951555, Los Angeles, CA 90095-1555, U.S.A. sjo@math.ucla.edu

Thus the minimization functional (1.1) can be reformulated in terms of the level set function $\phi(x)$ as

$$F(\phi, c_1, c_2) = \min_{\phi, c_1, c_2} \begin{array}{l} \int_D (f - c_1)^2 H(\phi)\, dx + \int_D (f - c_2)^2 (1 - H(\phi))\, dx \\ +\mu \int_D |\nabla H(\phi)| dx, \end{array} \tag{1.2}$$

where $H(x)$ is the heaviside function. This minimization problem is solved by taking the Euler-Lagrange equations and update the level set function $\phi(x)$ by the gradient descent method,

$$\phi_t = -\delta(\phi)((f - c_1)^2 - (f - c_2)^2 - \mu \nabla \cdot \frac{\nabla \phi}{|\nabla \phi|}), \tag{1.3}$$

where $\delta(x)$ is the delta function and the constants c_1 and c_2 are updated at each iteration by

$$c_1 = \frac{\int_D f H(\phi(x))\, dx}{\int_D H(\phi(x))\, dx},\ c_2 = \frac{\int_D f(1 - H(\phi(x)))\, dx}{\int_D (1 - H(\phi(x)))\, dx}. \tag{1.4}$$

The main drawback of solving this nonlinear parabolic PDE (1.3) is the computation expense due to the numerical stability constraint, i.e., the CFL condition.

To overcome the difficulty of solving the nonlinear PDE, Gibou and Fedkiw made an observation of (1.3) that only the zero level set of the function $\phi(x)$ is important. So they neglect the term $\delta(\phi)$ and replace the length term by a nonlinear diffusion preprocessing step. Thus they end up to solve the following ODE

$$\phi_t = -(f - c_1)^2 + (f - c_2)^2, \tag{1.5}$$

where c_1 and c_2 are updated according to (1.4). This converges very fast since a large time step can be taken. They also draw a connection between (1.5) and the k-means procedure (cf. [17]). However, in our work, we will link (1.3) with the topological derivative, which has been studied in our previous work [12] to the application of structural optimal design. So this paper can also be considered as a series work of different applications of the topological derivative.

Independently, Song and Chan [25] take a different approach to solve the Chan-Vese model. They go straightforward to the variational energy (1.1) or (1.2) without the length term. They compute the difference of the energy functional when they move a pixel x from inside the zero level set to outside (or vice versa). If the energy does not decrease, the pixel is kept inside; otherwise, it's favorable to move the pixel outside. To move a pixel cross the zero level set, they just simply replace $\phi(x)$ by $-\phi(x)$. This algorithm converges within a few iterations.

Based on [25], in Section 2 we introduce a fast algorithm by calculating a variational energy under the the multiphase level set framework. Therefore we are able to deal with complex images with triple junctions, multiple layers and etc. Two simple examples are shown to demonstrate the robustness and the efficiency of our fast algorithm. In Section 3, we make a connection between the idea behind this fast algorithm and the concept of the topological derivative. Furthermore, by applying topological derivative on the level set method (cf. [4, 12]), we make a link to the work in [25]. In addition, we take a preprocessing step (cf. [25]) to include the length term. In Section 4, we present more numerical examples to illustrate how our algorithm works in more complicated applications, which include noisy images and medical images. They all converge in less than 3 iterations.

Last but not the least, we want to mention a series of paper on image segmentation by different kinds of PDE based level set methods, such as the multilayer level set approach [8, 9] and piecewise constant level set methods [16, 15]. It would be interesting to compare our algorithm with theirs regarding to the speed, the quality of segmented results and the sensitivity to initial conditions and noise. This could be our future work.

2. Our Fast Algorithm.

2.1. The Two Level Set Framework. To segment images with multiple objects and/or junctions, we can easily generalize the above single level set method to a multiphase level set method [28]. Particularly here we use a two level set method with the functions denoted as ϕ_1 and ϕ_2. Thus we can segment any image up to four disjoint "color" regions, given by $\Omega_{11} := \{\phi_1 > 0, \phi_2 > 0\}$, $\Omega_{12} := \{\phi_1 > 0, \phi_2 < 0\}$, $\Omega_{21} := \{\phi_1 < 0, \phi_2 > 0\}$ and $\Omega_{22} := \{\phi_1 < 0, \phi_2 < 0\}$. Thus we define the associated energy functional without the length term as the following

$$\begin{aligned} F(\phi_1, \phi_2, \vec{c}) = \min_{\phi_1, \phi_2, \vec{c}} \quad & \int_D (f - c_{11})^2 H(\phi_1) H(\phi_2)\, dx \\ + \quad & \int_D (f - c_{12})^2 H(\phi_1)(1 - H(\phi_2))\, dx \\ + \quad & \int_D (f - c_{21})^2 (1 - H(\phi_1)) H(\phi_2)\, dx \\ + \quad & \int_D (f - c_{22})^2 (1 - H(\phi_1))(1 - H(\phi_2))\, dx, \end{aligned} \tag{2.1}$$

where the four constants c_{11}, c_{12}, c_{21} and c_{22} are computed as the following

$$\begin{aligned} c_{11} &= \frac{\int_D f H(\phi_1) H(\phi_2)\, dx}{\int_D H(\phi_1) H(\phi_2)\, dx}, & c_{12} &= \frac{\int_D f H(\phi_1)(1-H(\phi_2))\, dx}{\int_D H(\phi_1)(1-H(\phi_2))\, dx}, \\ c_{21} &= \frac{\int_D f (1-H(\phi_1)) H(\phi_2)\, dx}{\int_D (1-H(\phi_1)) H(\phi_2)\, dx}, & c_{22} &= \frac{\int_D f (1-H(\phi_1))(1-H(\phi_2))\, dx}{\int_D (1-H(\phi_1))(1-H(\phi_2))\, dx}. \end{aligned} \tag{2.2}$$

2.2. The Algorithm. The idea of our fast algorithm is that for any pixel $x_0 \in D$, we consider the variation of the energy functional (2.1) corresponding to move x_0 to any of the other three regions except the one x_0 belongs to. If the energy does not decrease, we keep x_0 at the current region; otherwise, we move x_0 to the one decreases most.

For the sake of clarity, we can write $F(\phi_1, \phi_2, \vec{c})$ in terms of the four regions $F(\Omega_{11}, \Omega_{12}, \Omega_{21}, \Omega_{22})$. This notation will be used in this subsection. We denote the number of pixels in the region of Ω_{11} as m_{11}, correspondingly the number of pixels in the region of Ω_{12}, Ω_{21} and Ω_{22} as m_{12}, m_{21} and m_{22}. We further assume that the area of a pixel occupies, i.e., the are of a grid, is 1. Then the constants defined in (2.2) can be rewritten as

$$\begin{aligned} c_{11} &= \frac{\int_{\Omega_{11}} f\, dx}{m_{11}}, & c_{12} &= \frac{\int_{\Omega_{12}} f\, dx}{m_{12}}, \\ c_{21} &= \frac{\int_{\Omega_{21}} f\, dx}{m_{21}}, & c_{22} &= \frac{\int_{\Omega_{22}} f\, dx}{m_{22}}. \end{aligned} \tag{2.3}$$

We consider the case of moving the pixel $x_0 \in \Omega_{11}$ to the region Ω_{12}. Denote the average of the new regions $\Omega_{11} - x$ and $\Omega_{12} + x$ correspondingly as $\bar{c}_{11}$ and $\bar{c}_{12}$, we have

$$\begin{aligned} \bar{c}_{11} &= \frac{\int_{\Omega_{11}-x_0} f\, dx}{m_{11}-1} &= c_{11} - \frac{f(x_0)-c_{11}}{m_{11}-1}, \\ \bar{c}_{12} &= \frac{\int_{\Omega_{12}+x_0} f\, dx}{m_{12}+1} &= c_{12} + \frac{f(x_0)-c_{12}}{m_{12}+1}. \end{aligned} \tag{2.4}$$

Then the variation of energy functional (2.1) from this action is computed below,

$$\begin{aligned} & F(\Omega_{11}-x_0,\Omega_{12}+x_0,\Omega_{21},\Omega_{22})-F(\Omega_{11},\Omega_{12},\Omega_{21},\Omega_{22}) \\ = & \int_{\Omega_{11}-x_0}(f-\bar{c}_{11})^2\,dx-\int_{\Omega_{11}}(f-c_{11})^2\,dx \\ & +\int_{\Omega_{12}+x_0}(f-\bar{c}_{12})^2\,dx-\int_{\Omega_{12}}(f-c_{12})^2\,dx \\ = & \int_{\Omega_{11}-x_0}(f-c_{11})^2\,dx-\tfrac{(f(x_0)-c_{11})^2}{m_{11}-1}-\int_{\Omega_{11}}(f-c_{11})^2\,dx \\ & +\int_{\Omega_{12}+x_0}(f-c_{12})^2\,dx-\tfrac{(f(x_0)-c_{12})^2}{m_{12}+1}-\int_{\Omega_{12}}(f-c_{12})^2\,dx \\ = & -\tfrac{m_{11}}{m_{11}-1}(f(x_0)-c_{11})^2+\tfrac{m_{12}}{m_{12}+1}(f(x_0)-c_{12})^2. \end{aligned} \tag{2.5}$$

Similarly, we can obtain the variations of the energy functional (2.1) from moving x_0 to the other two regions, Ω_{21} or Ω_{22}. They are

$$\begin{aligned} & F(\Omega_{11}-x_0,\Omega_{12},\Omega_{21}+x_0,\Omega_{22})-F(\Omega_{11},\Omega_{12},\Omega_{21},\Omega_{22}) \\ = & -\tfrac{m_{11}}{m_{11}-1}(f(x_0)-c_{11})^2+\tfrac{m_{21}}{m_{21}+1}(f(x_0)-c_{21})^2, \\ & F(\Omega_{11}-x_0,\Omega_{12},\Omega_{21},\Omega_{22}+x_0)-F(\Omega_{11},\Omega_{12},\Omega_{21},\Omega_{22}) \\ = & -\tfrac{m_{11}}{m_{11}-1}(f(x_0)-c_{11})^2+\tfrac{m_{22}}{m_{22}+1}(f(x_0)-c_{22})^2. \end{aligned} \tag{2.6}$$

Thus for the pixel $x_0 \in \Omega_{11}$, we first find the smallest value among the following four values : $\frac{m_{11}}{m_{11}-1}(f(x_0)-c_{11})^2$, $\frac{m_{12}}{m_{12}+1}(f(x_0)-c_{12})^2$, $\frac{m_{21}}{m_{21}+1}(f(x_0)-c_{21})^2$ and $\frac{m_{22}}{m_{22}+1}(f(x_0)-c_{22})^2$. Then we move x_0 to the corresponding region, denote it as Ω_{ij}. If this corresponding region Ω_{ij} is not the original one Ω_{11}, then we need to change $\phi_1(x_0)$ and $\phi_2(x_0)$ based on the sign of these both level set functions represented by Ω_{ij}. For example, if $i=1$ and $j=2$ then we just replace $\phi_2(x_0)$ by $-\phi_2(x_0)$. Furthermore, we need to update the constants c_{11} and c_{ij} following (2.4). Until now we can advance to the next pixel in some prescribed order. For example, in our numerical experiments, we sweep the pixels row by row. One iteration is finished when we have swept all the pixels in the image once. Usually less than 3 iterations are needed before the energy F remains unchanged.

2.3. Examples. In Figure 2.1 and Figure 2.2, two simple examples are presented to demonstrate the efficiency and the robustness of our fast algorithm compared with the results from multiphase PDE based level set methods [28].

In Figure 2.1, the first row shows the initial condition used for the both approaches. The second row shows our result which converges after only one iteration. The third row shows the result obtained from the PDE based method. This result is computed over 500 iterations and it gets stuck in a local minimum. From the first two images at the second row we observe that the square is split into two regions Ω_{11} and Ω_{12}. This is because an optimal solution obtained from our algorithm does not allow any of the four regions to be empty. For example, if Ω_{12} is empty, i.e., $m_{12}=0$, then according to (2.5), the energy functional F at the new shape $(\Omega_{11}-x_0,\Omega_{12}+x_0,\Omega_{21},\Omega_{22})$ is less than the energy functional F at the old shape $(\Omega_{11},\Omega_{12},\Omega_{21},\Omega_{22})$. Therefore the shape $(\Omega_{11},\Omega_{12},\Omega_{21},\Omega_{22})$ with an empty region Ω_{12} can not be an optimal solution. However this argument does not affect the segmented result, see the last image at the second row.

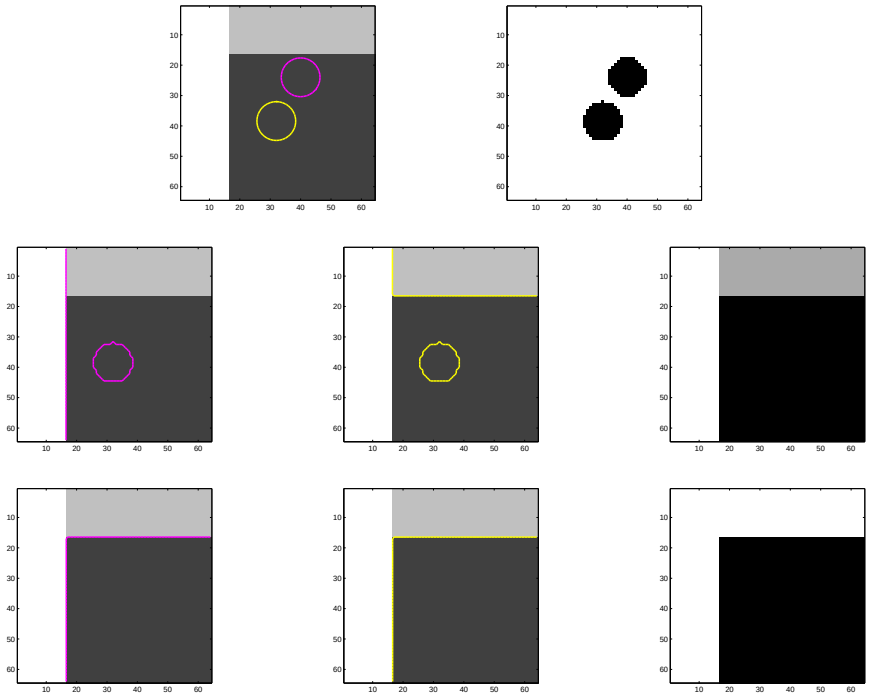

FIG. 2.1. *A simple example of triple junction. The first row: the initial condition. The second row: the result from our algorithm. The third row: the result from PDE based level set methods. Left: the zero level set of ϕ_1; Middle: the zero level set of ϕ_2; Right: segmented regions.*

Figure 2.2 shows four different initial conditions used for our both approaches. Our fast algorithm converges correctly within 2 iterations for the first three initial conditions but the bottom right initial condition. In that case, our algorithm gets stuck at the outer circle. This is simply because three initial regions (Ω_{11}, Ω_{12} and Ω_{21}) all belong to the black background. However, none of the four initial conditions works for the PDE based method. They all converge to the same local minimum trapped at the outer circle. This is because that the PDE based level set method evolves level sets mainly near the zero level set. When a pixel is far away from the zero level set, it is not likely to cross over it. We will comment on this more in the next section after we introduce the concept of the topological derivative.

Remark 1 *Strictly speaking, our fast algorithm does not use the level set evolution. More precisely, we only use the level set method to formulate our problem.*

Remark 2 *Since the level set function values and the constants are updated along with the sweeping procedure, the sweeping order should matter. This is usually an issue of Gauss Seidel iteration. However in our case, it is easier to just choose a different initial condition than a different sweeping order.*

3. The Connection to the Topological Derivative. Let us go back to (1.4), where both constants c_1 and c_2 are correspondingly defined as the average of the image f inside or outside the subset Ω. Therefore we can rewrite the minimization

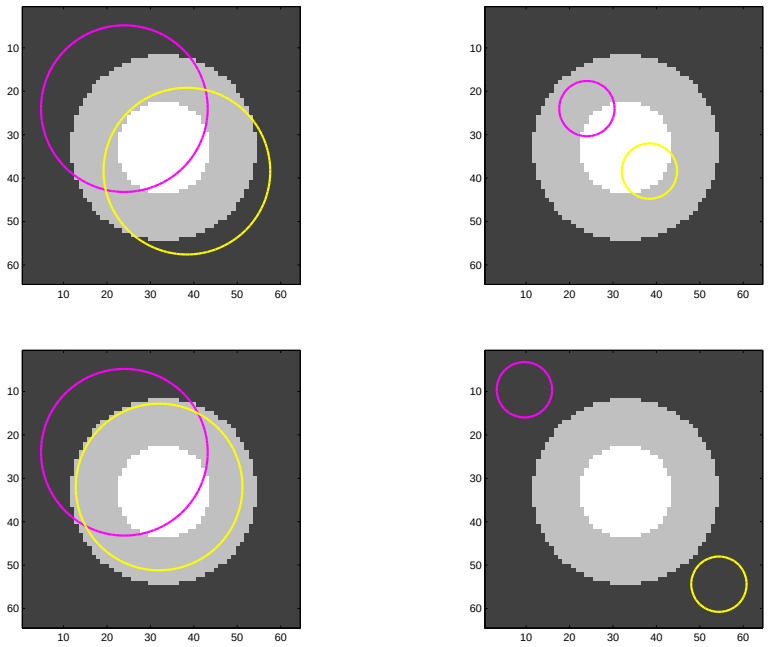

FIG. 2.2. *Four different initial conditions used for comparisons between our fast algorithm and multiphase PDE based level set methods.*

problem (1.1) or (1.2) as

$$F(\Omega) = \min_{\Omega} \int_{\Omega} (f - c_1(\Omega))^2 \, dx + \int_{D\setminus\Omega} (f - c_2(\Omega))^2 \, dx + \mu \int_{\partial\Omega} ds, \tag{3.1}$$

where again, $c_1(\Omega) = \frac{\int_\Omega f \, dx}{\int_\Omega dx}$ and $c_2(\Omega) = \frac{\int_{D\setminus\Omega} f \, dx}{\int_{D\setminus\Omega} dx}$.

Originally, the Chan-Vese model (1.1) or (1.2) is defined as a minimization problem determined by the shape of Ω and two constants c_1 and c_2. Now with this new form (3.1), the active contour model becomes a pure shape optimization problem, where a huge literature [20, 24, 2, 1] can be accessed from the shape optimization field. Particularly in our work, the concept of the topological derivative [23, 10, 3] is employed to explain why our algorithm works efficiently and robustly.

3.1. The Topological Derivative. The idea of the topological derivative is to create a small ball $B_{\rho,x}$ with center x and radius ρ inside/outside the domain Ω and then consider the variation of the objective functional $\mathcal{F}$ with respect to the volume of this small ball. For $x \in \overline{\Omega}$, the topological derivative $d_{\mathcal{T}}\mathcal{F}(\Omega)(x)$ is defined as the limit (if it exists)

$$d_{\mathcal{T}}\mathcal{F}(\Omega)(x) := \lim_{\rho\to 0} \frac{\mathcal{F}(\Omega_{\rho,x}) - \mathcal{F}(\Omega)}{|B_{\rho,x} \bigcap \Omega|}, \tag{3.2}$$

where $\Omega_{\rho,x} = \Omega - \overline{B(\rho, x)}$. Thus to minimize the energy functional $\mathcal{F}$, a hole should be created at the point x if the topological derivative is negative. This is clearly the

same idea as our fast algorithm, which now can be considered as a discrete application of the topological derivative.

The above definition of the topological derivative is based on two regions Ω and $D \setminus \Omega$. Nevertheless it can be generalized to multiple regions as the following. For $x \in \Omega_{11}$, if we create a small hole of $B_{\rho,x}$ and add it to the region Ω_{12}, then with the notation of

$$\begin{array}{rcccl} c_{11}^{\rho} & = & \frac{\int_{\Omega_{11}-B(\rho,x)} f dxdy}{\int_{\Omega_{11}-B(\rho,x)} dxdy} & = & c_{11} - \frac{\int_{B(\rho,x)} (f-c_{11})\, dx}{|\Omega_{11}|-\pi\rho^2} \\ c_{12}^{\rho} & = & \frac{\int_{\Omega_{12}+B(\rho,x)} f dxdy}{\int_{\Omega_{12}+B(\rho,x)} dxdy} & = & c_{12} + \frac{\int_{B(\rho,x)} (f-c_{12})\, dx}{|\Omega_{12}|+\pi\rho^2}, \end{array} \tag{3.3}$$

the topological derivative of this perturbation is computed as follows,

$$\begin{aligned} & \lim_{\rho\to 0} \frac{\int_{\Omega_{11}-B(\rho,x)} (f-c_{11}^{\rho})^2 dxdy - \int_{\Omega_{11}} (f-c_{11})^2 dxdy}{\pi\rho^2} \\ & + \lim_{\rho\to 0} \frac{\int_{\Omega_{12}+B(\rho,x)} (f-c_{12}^{\rho})^2 dxdy - \int_{\Omega_{12}} (f-c_{12})^2 dxdy}{\pi\rho^2} \\ = & \lim_{\rho\to 0} \frac{\int_{\Omega_{11}-B(\rho,x)} (f-c_{11})^2 dxdy - \frac{(\int_{B(\rho,x)} (f-c_{11})\, dx)^2}{|\Omega_{11}|-\pi\rho^2} - \int_{\Omega_{11}} (f-c_{11})^2 dxdy}{\pi\rho^2} \\ & + \lim_{\rho\to 0} \frac{\int_{\Omega_{12}+B(\rho,x)} (f-c_{12})^2 dxdy - \frac{(\int_{B(\rho,x)} (f-c_{12})\, dx)^2}{|\Omega_{12}|+\pi\rho^2} - \int_{\Omega_{12}} (f-c_{12})^2 dxdy}{\pi\rho^2} \\ = & \begin{cases} -(f(x)-c_{11})^2 + (f(x_0)-c_{12})^2, & \text{if } |\Omega_{12}| > 0; \\ -(f(x)-c_{11})^2, & \text{if } |\Omega_{12}| = 0. \end{cases} \end{aligned} \tag{3.4}$$

Similarly, we obtain the topological derivative of creating a hole centered at x in Ω_{11} and add it to Ω_{21} or Ω_{22}. Comparing (3.4) with the expressions (2.5) and (2.6) in Section 2.2., we see indeed that our fast algorithm is based on a discrete definition of the topological derivative. The rigorous definition given here uses a hole with the area $\pi\rho^2$ and $\rho \to 0$, while the discrete definition replaces that by a grid with the area equals 1.

3.2. A Connection to the Work of Gibou and Fedkiw. To draw a connection between the topological derivative and the work in [11], we will go back to the single level set framework again. Following the analysis of (3.4), we obtain the topological derivative of the objective functional F with the shape functional Ω for $x_0 \in \Omega$ is $-(f(x_0)-c_1)^2 + (f(x_0)-c_2)^2$ and for $x_0 \in D \setminus \Omega$ is $(f(x_0)-c_1)^2 - (f(x_0)-c_2)^2$. Based on these, to minimize the objective functional $\mathcal{F}$, we know (cf. [4, 12]):

- If $\phi(x_0) > 0$, and $-(f(x_0)-c_1)^2 + (f(x_0)-c_2)^2 > 0$, then it is not favorable to generate a hole at x_0 which means the value of ϕ should not decrease.
- If $\phi(x_0) > 0$ and $-(f(x_0)-c_1)^2 + (f(x_0)-c_2)^2 < 0$, then the value of ϕ should decrease since it is favorable to generate holes.
- If $\phi(x_0) < 0$ and $(f(x_0)-c_1)^2 - (f(x_0)-c_2)^2 > 0$, then it's not favorable to create hole and thus the value of $\phi(x,t)$ should not increase.
- If $\phi(x_0) < 0$ and $(f(x_0)-c_1)^2 - (f(x_0)-c_2)^2 < 0$, then it's favorable to create a hole which means the value of ϕ should increase.

Then to obtain the minimizer of the objective functional (3.1) (equivalent to (1.1) and (1.2)) without the length term, we choose to solve the ODE (1.5), which satisfies the

above requirements. For more details, see [4, 12]. This leads to Gibou and Fedkiw's work in [11]. To solve (1.5), we can take a large time step. Or, we can just update the level set function $\phi(x)$ by the sign of $-(f(x)-c_1)^2+(f(x)-c_2)^2$ as follows,

$$\phi^{n+1}(x)=\begin{cases} 1 & \text{if } -(f(x)-c_1(\phi^n(x)))^2+(f(x)-c_2(\phi^n(x)))^2>0 \\ -1 & \text{else.} \end{cases} \tag{3.5}$$

This method updates ϕ by so called the Jordan iteration compared with the the Gauss Seidel iteration used by our fast algorithm. The method of updating ϕ by the Jordan iteration converges within a few iterations because whether a pixel x outside or inside the zero level set of ϕ is solely determined by the distance between the value of $f(x)$ and c_1 or c_2, see also [25]. This analogy can be trivially extended to the multiphase level set framework we use here. Thus it also explains why our algorithm based on the Gauss Seidel iteration converges so fast.

Up to now, we have linked [11] and [25] together through the topological derivative. And we mention here that those PDE based level set methods solved in [7, 28, 8, 9] can be considered as level set approaches based on shape derivatives [24]. As pointed out in [2, 1], the level set approach based on the shape sensitivity may get stuck at shapes with fewer holes than the optimal geometry in some applications to structure designs. This is also the case in image segmentation. Thus in the numerical experiments of those work mentioned above, initial conditions with many small circles are used. However, our algorithm together with [11, 25] do not have this problem. The advantage of applying the topological derivative on the level set method is the ability to create holes even far away from the zero level set.

3.3. The Length Term. By far, we have not mentioned how to deal with the length term. It is necessary particularly for noisy images or images with edges not defined by a gradient. To include the length term, special attentions are paid in [25, 11]. The authors of [25] apply several iterations of the PDE-based algorithm (1.3) to the obtained optimal solution from their fast algorithm. And the authors of [11] choose a preprocessing step on the given image f and then apply their algorithm to this processed image. The idea of this preprocessing step is to use isotropic nonlinear diffusion [22] for denoising images while still keeping the image edges intact. The nonlinear equation they solve is

$$I_t(x,t)=\nabla\cdot(g(|\nabla I|)\nabla I), \tag{3.6}$$

where $I(x,t)$ defines the image and g is an edge-stopping function such that $\lim_{s\to\infty} g(s)=0$, i.e., diffusion stops at the location of large gradients.

The reason why they treat the length term different are not given in their work. Now based on the topological derivative, we know it is because the topological derivative of the objective functional $\mathcal{F}(\Omega)=|\partial\Omega|$ does not exist. In fact,

$$d_{\mathcal{T}}|\partial\Omega|=\lim_{\rho\to 0}\frac{|\partial B_{\rho,x}|}{|B_{\rho,x}|}\simeq\lim_{\rho\to 0}\frac{\rho^{N-1}}{\rho^N}=\infty.$$

In our work, we also take the preprocessing step to re-introduce the notion of the scale term. Following [11], we choose $g(s)=\nu/(1+s^2/K^2)$, where ν is a parameter controlling the length scale and K is fixed as 7. We use the Alternative Direction Explicit (ADE) technique to solve (3.6), see [14]. We only conduct a few iterations of (3.6) since our intention is not to denoise but to segment the image f.

4. More Numerical Examples. First in Figure 4.1, we show two segmentation results from a noise free image and the same image with an added Gaussian noise. The preprocessing step is taken for the noisy image with $\nu = 1$ and 5 ADE iterations. The convergence of the fast algorithm for the both images is within 2 iterations. We note that our algorithm plus the preprocessing step is not sensitive to the noise. Even though the right triangle does not have a sharp contrast with the background and noise, the optimal solution still finds it correctly.

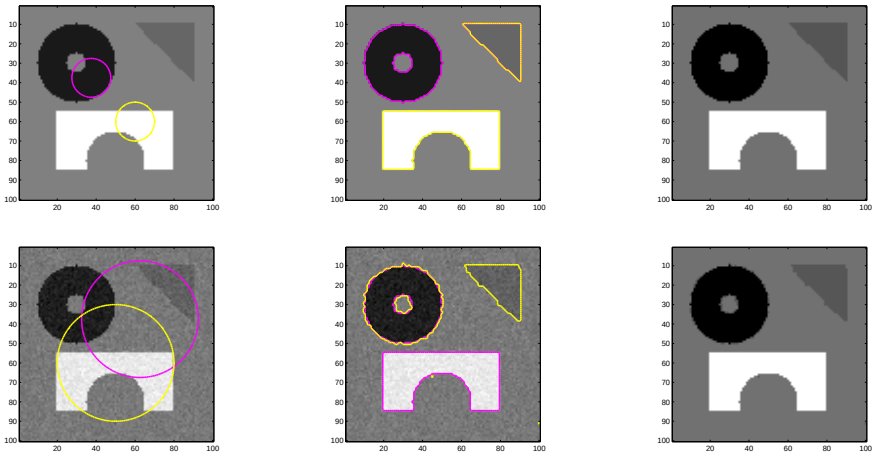

FIG. 4.1. *Segmentation of a noise free image and a noisy image. Left: the initial condition; Middle: zero level sets of ϕ_1 and ϕ_2 ; Right: the segmented result.*

Then in Figure 4.2 we present a tricky example to show that our fast algorithm is sometimes sensitive to initial conditions. The synthetic image in Figure 4.2 is composed of 5 piecewise constant parts with the gray value of the outer 3/4 circle is exactly the mean of the gray value of the left square and the gray value of the center square besides the inner circle. Therefore it is very likely that the optimal solution does not distinct the center square from the 3/4 circle. See the bottom images.

We conclude our paper by showing how our algorithm works on medical images in the next three figures. For each image, a preprocessing step is taken and the fast algorithm converges within 2 iterations. We notice that the zero level sets of ϕ_1 and ϕ_2 overlap sometimes since there is no restriction on the length of both interfaces. Nevertheless, the segmented results are still good. see Figure 4.3, Figure 4.4 and Figure 4.5.

REFERENCES

[1] G. Allaire, F. Jouve, and A.M. Toader. Structural optimization using sensitivity analysis and a level-set method. *J. Comput. Phys.*, 194(1):363–393, 2004.

[2] Gregoire Allaire, Francois Jouve, and Anca-Maria Toader. A leve-set method for shape optimization. *C.R. Acad. Sci. Paris, Ser. I*, 334:1125–1130, 2002.

[3] Samuel Amstutz and Heiko Andrae. A new algorithm for topology optimization using a level-set method. *J. Comp. Phys.*, 216:573–588, 2006.

[4] M. Burger, B. Hackl, and W. Ring. Incorporating topological derivatives into level set methods. *J. Comp. Phys*, 194:344–362, 2004.

[5] V. Caselles, F. Catte, T. Coll, and F. Dibos. A geometric model for active contours in image processing. *Numerische Mathematik*, 66:1–31, 1993.

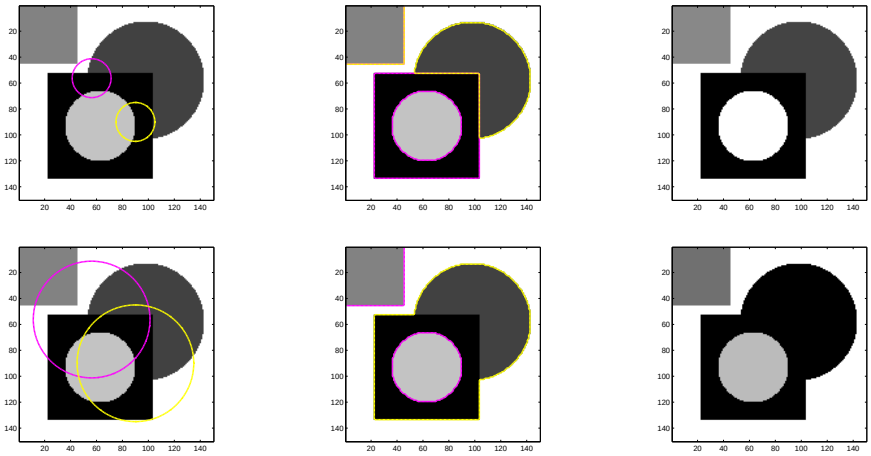

FIG. 4.2. *Segmentation of a synthetic image. Top: an example that our algorithm works; Bottom: an example that our algorithm does not work. Left: the initial condition; Middle: zero level sets of* ϕ_1 *and* ϕ_2 *; Right: the segmented result. No preprocessing step is taken.*

[6] V. Caselles, R. Kimmel, and G. Sapiro. Geodesic active contours. *International Journal of Computer Vision*, 22(1):61–79, 1997.

[7] T. Chan and L. Vese. Active contours without edges. *IEEE Transations on Image Processing*, 10(2):266–277, 2001.

[8] Ginmo Chung and Luminita Vese. Image segmentation using a multilayer level set approach. Technical Report 03-53, UCLA, 2003.

[9] Ginmo Chung and Luminita Vese. Energy minimization based segmentation and denoising using multilayer level set approach. volume 3457/2005, pages 439–455. EMMCVPR, 2005. LNCS Vol. 3757/2005.

[10] Stephane Garreau, Philippe Guillaume, and Mohamed Masmoudi. The topological asymptotic for PDE systems: The elasticity case. *SIAM J. Control Optim.*, 39:1756–1778, 2001.

[11] Frederic Gibou and Ronald Fedkiw. Fast hybrid k-means level set algorithm for segmentation. In *The Procedings of the 4th Annual Hawaii International Conference on Statistics and Mathematics*, 2002. Stanford Technical Report, Nov 2002.

[12] Lin He, Chiu-Yen Kao, and Stanley Osher. Incorporating topological derivatives into shape derivatives based level set methods. UCLA CAM Report 06-44, 2006.

[13] S. Kichenassamy, A. Kumar, P. Olver, A. Tannenbaum, and Z. Yezzi. Gradient flows and geometric active contour models. *ICCV*, 1995.

[14] S. Leung and S. Osher. Global minimization of the active contour model with TV-inpainting and two-phase denoising. *Lecture Notes in Computer Science*, 3752:149–160, 2005.

[15] Hongwei Li and Xue-Cheng Tai. Piecewise constant level set methods for multiphase motion. *International Journal of Numerical Analysis and Modeling*, 4:291–305, 2007.

[16] Johan Lie, Marius Lysaker, and Xue-Cheng Tai. *Piecewise Constant Level Set Methods and Image Segmentation*, volume 3459 of *Lecture Notes in Computer Science*, pages 573–584. Springer Berlin / Heidelberg, 2005.

[17] J. MacQueen. Some methods for classification and analysis of multivariate observation. In *Proceedings of the Fifth Berkeley Symposium on Mathematical Satistics and Probability*, pages 281–297, 1967.

[18] R. Malladi, J.A. Sethian, and B.C. Vemuri. Shape modeling with front propagation: A level set approach. *IEEE Transactions on Pattern Analysis and Machine Intelligence*, 17(2):158–175, 1995.

[19] D. Mumford and J. Shah. Optimal approximation by piecewise smooth functions and associated variational problems. *Comm. Pure Appl. Math*, 42:577–685, 1989.

[20] F. Murat and S. Simon. Etudes de problems d'optimal design. *Lectures Notes in Computer Science*, 41:54–62, 1976.

[21] Stanley Osher and James A. Sethian. Fronts propagating with curvature dependent speed; algorithms based on hamilton-jacobi formulations. *J. Comput. Phys.*, 79:12–49, 1988.

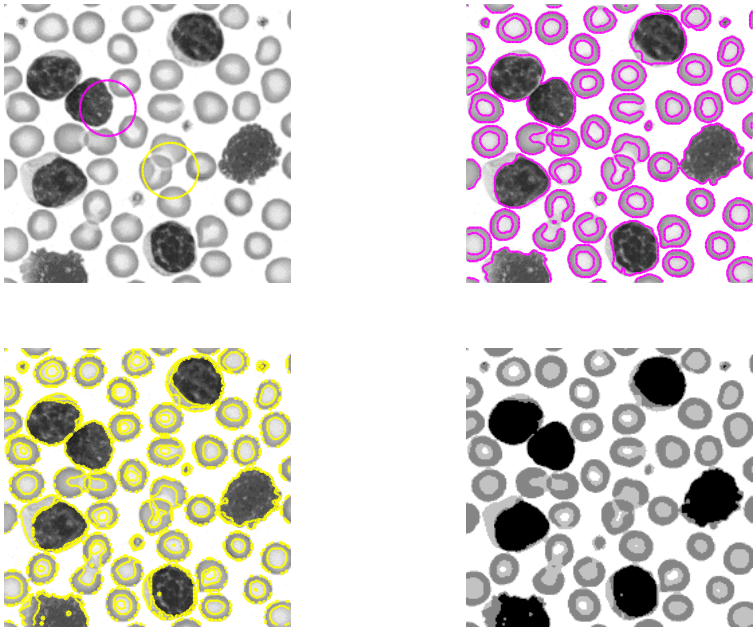

FIG. 4.3. *Segmentation of blood cells. Top left: the initial condition; Top right: the zero level set of ϕ_1; Bottom left: the zero level set of ϕ_2; Bottom right: the segmented result. $\nu = 1.0$, 5 ADE iterations are solved.*

[22] P. Perona and J. Malik. Scale-space and edge detection using anisotropic diffusion. *IEEE Trans. PAMI*, 12(7):629–639, 1990.

[23] J. Sokolowski and A. Zochowski. On the topological derivative in shape optimization. *SIAM J. Control Optim.*, 37:1251–1272, 1999.

[24] J. Sokolowski and J.-P. Zolesio. *Introduction to Shape Optimization: Shape Sensitivity Analysis.* Springer, Heidelberg, 1992.

[25] Bing Song and Tony Chan. A fast algorithm for level set based optimization. CAM 02-68, UCLA, December 2002.

[26] D. Terzopoulos and K. Fleischer. Deformable models. *The Visual Computer*, 4(6):306–331, 1988.

[27] D. Terzopoulos, J. Platt, A. Barr, and K. Fleischer. Elastically deformable models. In *Comp. Graphics Proc.*, pages 205–214. ACM Press/ ACM SIGGRAPH, 1987.

[28] Luminita Vese and Tony Chan. A multiphase level set framework for image segmentation using the mumford and shah model. *International Journal of Computer Vision*, 50(3):271–293, 2002.

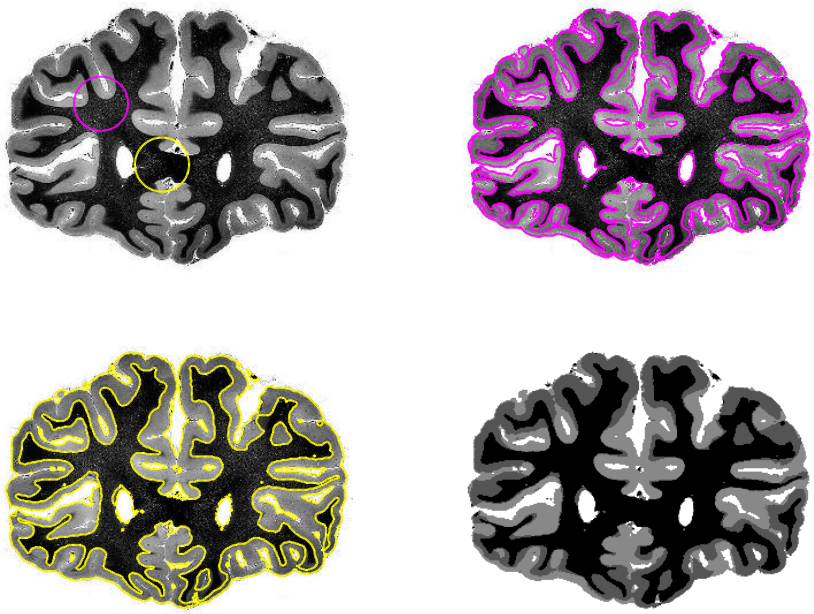

FIG. 4.4. *Segmentation of a brain data. Top left: the initial condition; Top right: the zero level set of ϕ_1; Bottom left: the zero level set of ϕ_2; Bottom right: the segmented result. $\nu = 2.0$, 5 ADE iterations are solved.*

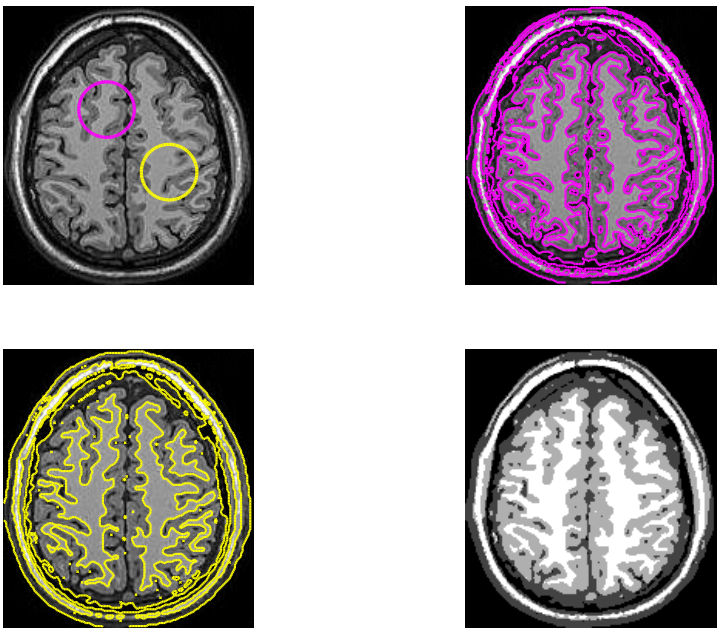

FIG. 4.5. *Segmentation of a brain data. Top left: the initial condition; Top right: the zero level set of ϕ_1; Bottom left: the zero level set of ϕ_2; Bottom right: the segmented result. $\nu = 1.0$, 5 ADE iterations are solved.*